RAA 2021 Vol. **21** No. **8**, 199(8pp) doi: 10.1088/1674-4527/21/8/199

http://www.raa-journal.org *http://iopscience.iop.org/raa*

Research in Astronomy and Astrophysics

X-ray spectral evolution in an X-ray changing-look AGN NGC 1365 with variable column density

Hao Liu[1], Qing-Wen Wu[1], Yong-Quan Xue[2,3], Ting-Gui Wang[2,3], Jun Yang[4], Heng-Xiao Guo[5] and Zhi-Cheng He[2,3]

[1] Department of Astronomy, School of Physics, Huazhong University of Science and Technology, Wuhan 430074, China; *qwwu@hust.edu.cn*

[2] CAS Key Laboratory for Research in Galaxies and Cosmology, Department of Astronomy, University of Science and Technology of China, Hefei 230026, China

[3] School of Astronomy and Space Science, University of Science and Technology of China, Hefei 230026, China

[4] Department of Space, Earth and Environment, Chalmers University of Technology, Onsala Space Observatory, SE-439 92 Onsala, Sweden

[5] Department of Physics and Astronomy, 4129 Frederick Reines Hall, University of California, Irvine, CA, 92697-4575, USA

Received 2021 March 9; accepted 2021 March 31

Abstract X-ray changing-look active galactic nuclei (CL AGNs) are a subpopulation of AGNs, whose line-of-sight column densities increase/decrease within several years. The physical mechanism for the variation of column density is unclear. We reduce the X-ray data from XMM-Newton and NuSTAR observations for a CL AGN NGC 1365 with strong variation of column densities. The X-ray spectrum quickly softens as the X-ray luminosity increases and optical-to-X-ray spectral index also increases as increasing of optical luminosity. These results support that NGC 1365 also undergoes strong spectral evolution as that recently suggested for the optically selected CL AGNs with reappearance/disappearance of broad emission lines. Therefore, the variation of column density may be driven by the variable disk winds during the strong evolution of disk/corona.

Key words: galaxies: active — galaxies: Seyfert — quasars: emission lines — accretion, accretion disks

1 INTRODUCTION

An active galactic nucleus (AGN) is powered by accretion of matter onto the supermassive black hole (SMBH) that is located at the center of a galaxy. The unification model is proposed to explain the main properties of the large zoo of AGNs. The obscuring torus plays a key role in the unification model, where both broad emission lines and narrow lines are observed in type 1 AGNs while the broad lines are obscured by the torus in type 2 AGNs due to large viewing angles (Antonucci 1993; Urry & Padovani 1995). The obscuring material can have a sufficiently high column density (i.e., $N_{\rm H} > 10^{24}{\rm cm}^{-2}$), and even the hard X-ray emission can be significantly obscured. Recently, many observations at different wavebands have challenged the dichotomy of the AGNs in the unification model. The so-called changing-look (CL) AGN is a term first used to classify AGNs that showed an extreme variation in X-ray column density, which showed rapid transitions between Compton-thin ($N_{\rm H} < 10^{24}{\rm cm}^{-2}$) and Compton-thick ($N_{\rm H} > 10^{24}{\rm cm}^{-2}$) regimes (hereafter X-ray-selected CL AGNs, e.g., Ricci et al. 2016, and references therein). The second type of CL AGNs is defined through optical observations that show transitions between optical spectral types from type 1 to intermediate type (types 1.8 and 1.9) to type 2, or vice versa within several years or even shorter (hereafter optically selected CL AGNs, e.g., Trippe et al. 2008; Denney et al. 2014; Kim et al. 2018). Traditionally, the CL phenomenon was considered to be rare. However, the number of CL AGNs grew rapidly in last few years with more and more optical and X-ray surveys (e.g., MacLeod et al. 2016; Ruan et al. 2016; Yang et al. 2018; Mathur et al. 2018; MacLeod et al. 2019; Trakhtenbrot et al. 2019; Guo et al. 2019, 2020).

Several models have been proposed to explain the physical mechanism of the changing-look phenomenon. Due to the quite short timescale of CL within few years or even months, it was proposed that the CL may be caused by the variation of absorbing material that moves in or moves out of the line of sight, where the broad emission lines in AGNs will disappear or reappear. This absorber-motion scenario is supported by the fact that the column density of a CL AGN varies quickly (e.g., Goodrich 1989; Tran et al. 1992; Risaliti et al. 2009). However, many CL AGNs show little absorption or only weak absorption, which contradicts with the absorber-motion scenario (e.g., Rivers et al. 2012; McElroy et al. 2016; Noda & Done 2018). The CL AGNs show the quite low polarization in optical linear polarization measurements, which suggests that the transition from type 1 to type 2 cannot be attributed to the putative dust obscuration (e.g., Hutsemékers et al. 2019). Sheng et al. (2017) found large variations in the mid-infrared luminosity echoing the optical variations that occur during the change look of AGNs, which is also not consistent with the obscuration scenario and supports that the CL may be caused by the intrinsic variation of accretion process. The rapid variation of CL may be similar to the state transition as found in stellar-mass black-hole binaries, which is driven by the accretion process (Noda & Done 2018). It should be noted that the short timescale of the CL also challenges the various instabilities of accretion disk. The radiation-pressure instability in a narrow region of the truncated disk and the action by a close binary of SMBHs are proposed to explain the observed timescales of the CL phenomenon (Śniegowska & Czerny 2019; Wang & Bon 2020).

NGC 1365 is a nearby obscured Seyfert (z=0.0055) with multiple hard X-ray observations, which is a prototype of CL AGNs that show the column density of the X-ray absorber changing from Compton-thin to Compton-thick (e.g., Ramos Almeida et al. 2009). Its X-ray luminosity showed rapid variability within several tens of seconds (e.g., Risaliti et al. 2009). Its optical observations revealed weak broad components of Hα and Hβ lines from 1979 to 2014, and it is defined as a Seyfert 1.8 or 1.9 (e.g., Edmunds & Pagel 1982; Schulz et al. 1999; Trippe et al. 2010; Schnorr-Müller et al. 2016). Its black hole mass is $5 \times 10^6 M_\odot$ and NGC 1365 has a moderate Eddington ratio (e.g., Onori et al. 2017; Fausnaugh et al. 2018). The central SMBH is spinning rapidly with a dimensionless spin rate of $a_* > 0.97$ as constrained from the broad Fe Kα line observed by XMM-Newton and NuSTAR (e.g., Walton et al. 2014).

It is still unclear why some AGNs show the changing-look behavior and what the difference between optically-selected and X-ray selected CL AGNs is. In this work, we explore these issues based on the analyses of X-ray and optical spectral evolution for NGC 1365 using the XMM-Newton and NuSTAR observations. In Section 2, we present the data reduction for NGC 1365. The main results, discussions and conclusions are presented in Sections 3, 4 and 5, respectively. For this work, we adopt a cosmological model of $\Omega_m = 0.32$, $\Omega_\Lambda = 0.68$, and $H_0 = 67\,{\rm km\ s^{-1}\ Mpc^{-1}}$ (Planck Collaboration et al. 2014).

2 DATA REDUCTION

2.1 XMM-Newton Data

NGC 1365 had been observed by XMM-Newton during 2003-2013. In this work, we selected eight observations with observing time longer than 10 kilo-seconds. The observations in 2007 were not considered, where they showed a reflection-dominated spectrum below 10 keV due to $N_{\rm H} \sim 10^{24-25}{\rm cm}^{-2}$ and the intrinsic X-ray spectrum cannot be well constrained with XMM-Newton observations. All the selected data were reduced using the Science Analysis Software (SAS, version 18.0.0). The source spectra were extracted using a circular region with a radius of 10 arcseconds. The background spectra were extracted from source-free, nearby regions with the same size. We use the data from EPIC instrument in two modes of MOS and PN, where both MOS1 and MOS2 adopted. The spectra were analyzed by using standard software packages of HEASOFT (version 6.25). The X-ray emission of NGC 1365 contains significant extended emission from a circumnuclear starburst, as imaged by Chandra (Wang et al. 2009). This extended emission dominates the X-ray spectrum below $\sim$ 2 keV, while the spectrum above $\sim$ 3 keV is dominated by the AGN itself. Therefore, we considered the X-ray spectra in 3-10 keV in this work. The X-ray fitting results and corresponding parameters are presented in Table 1.

2.2 NuSTAR Data

NGC 1365 was also observed four times as part of the XMM-Newton and NuSTAR (Nuclear Spectroscopic Telescope Array) monitoring program, where the observations were performed simultaneously to provide the optimal broadband X-ray spectra to investigate the overall X-ray emission and spectral variability. These simultaneous observations also allow us to determine the reliability of the spectral fitting based on pure XMM-Newton observations. The data were reduced using the NuSTAR Data Analysis Software (nustardas v1.4.1), the CALDB (version 20150316) and standard filtering criteria with the *nupipeline* task. The spectra were extracted by the *nuproducts* task, where the source region and background region were selected as two circular regions with the same radius of 100 arcseconds which include and exclude the source, respectively. To compare with pure XMM-Newton observations, we select the data of joint NuSTAR observations which were obtained from the instruments FPMA and FPMB in 3-78 keV. Spectral analysis was performed using the software HEASOFT (version 6.25).

Table 1 X-ray Modeling Results of NGC 1365

ObsID	Date (YY-MM-DD)	Model	$N_{\rm H}/10^{22}$ (cm^{-2})	**GABS1** E_1/keV	σ_1/keV	**GABS2** E_2/keV	σ_2/keV	Γ	**LAOR** E/keV	$\log(L_{\rm 2-10keV}/L_{\rm Edd})$‡	χ^2/dof.
(1)	(2)	(3)	(4)	(5)	(6)	(7)	(8)	(9)	(10)	(11)	(12)
					XMM-Newton results						
0151370101	03-01-16	A	$23.23^{+3.10}_{-2.98}$	-	-	-	-	$1.29^{+0.22}_{-0.23}$	-	–2.89	482.64/390
0151370701	03-08-13	B	$23.40^{+5.08}_{-5.18}$	$7.02^{+0.03}_{-0.04}$	$0.01^{+0.04}_{-0.01}$	$6.71^{+0.03}_{-0.02}$	$0.06^{+0.04}_{-0.04}$	$1.74^{+0.43}_{-0.47}$	$5.93^{+0.07}_{-0.09}$	–2.66	311.35/313
0205590301	04-01-17	B	$14.22^{+0.73}_{-0.74}$	$7.05^{+0.02}_{-0.02}$	$0.10^{+0.05}_{-0.06}$	$6.69^{+0.02}_{-0.02}$	$0.08^{+0.01}_{-0.02}$	$2.46^{+0.09}_{-0.08}$	$6.05^{+0.06}_{-0.11}$	–2.41	2566.33/2603
0205590401	04-07-24	B	$17.18^{+1.93}_{-2.00}$	$7.11^{+0.02}_{-0.03}$	$0.15^{+0.04}_{-0.06}$	$6.74^{+0.03}_{-0.02}$	$0.06^{+0.03}_{-0.02}$	$1.55^{+0.17}_{-0.20}$	$6.18^{+0.04}_{-0.07}$	–2.75	1568.61/1496
0692840201	12-07-25	B	$18.27^{+0.88}_{-0.93}$	$7.00^{+0.04}_{-0.02}$	$0.05^{+0.01}_{-0.01}$	$6.70^{+0.01}_{-0.04}$	$0.07^{+0.02}_{-0.03}$	$1.50^{+0.08}_{-0.09}$	$5.90^{+0.16}_{-0.06}$	–2.65	1053.92/968
0692840301	12-12-24	B	$6.97^{+0.36}_{-0.41}$	$7.07^{+0.02}_{-0.02}$	$0.12^{+0.04}_{-0.04}$	$6.71^{+0.01}_{-0.02}$	$0.08^{+0.01}_{-0.01}$	$1.96^{+0.04}_{-0.05}$	$6.09^{+0.04}_{-0.06}$	–2.37	1365.99/1186
0692840401	13-01-23	B	$3.68^{+0.34}_{-0.38}$	$7.02^{+0.01}_{-0.02}$	$0.06^{+0.03}_{-0.05}$	$6.69^{+0.02}_{-0.01}$	$0.08^{+0.01}_{-0.02}$	$1.93^{+0.04}_{-0.04}$	$5.99^{+0.04}_{-0.05}$	–2.42	2032.00/1897
0692840501	13-02-12	B	$11.37^{+0.51}_{-0.53}$	$7.03^{+0.01}_{-0.01}$	$0.06^{+0.03}_{-0.03}$	$6.70^{+0.01}_{-0.01}$	$0.06^{+0.02}_{-0.02}$	$1.79^{+0.06}_{-0.05}$	$6.00^{+0.03}_{-0.04}$	–2.50	2118.30/2136
					XMM-Newton+NuSTAR results						
0692840201 60002046002	12-07-25	C	$18.42^{+0.47}_{-0.47}$	$7.00^{+0.05}_{-0.02}$	$0.06^{+0.01}_{-0.01}$	$6.69^{+0.02}_{-0.04}$	$0.07^{+0.02}_{-0.04}$	$1.62^{+0.02}_{-0.03}$	$5.94^{+0.15}_{-0.07}$	–2.63	1772.54/1672
0692840301 60002046005	12-12-24	C	$5.17^{+0.22}_{-0.22}$	$7.08^{+0.02}_{-0.02}$	$0.11^{+0.04}_{-0.04}$	$6.69^{+0.01}_{-0.02}$	$0.10^{+0.01}_{-0.02}$	$1.88^{+0.01}_{-0.02}$	$6.05^{+0.04}_{-0.04}$	–2.35	2874.49/2332
0692840401 60002046007	13-01-23	C	$1.71^{+0.21}_{-0.21}$	$7.02^{+0.02}_{-0.01}$	$0.06^{+0.03}_{-0.04}$	$6.69^{+0.02}_{-0.02}$	$0.10^{+0.02}_{-0.02}$	$1.85^{+0.01}_{-0.02}$	$5.97^{+0.03}_{-0.04}$	–2.40	3793.59/3069
0692840501 60002046009	13-02-12	C	$9.83^{+0.28}_{-0.27}$	$7.03^{+0.01}_{-0.01}$	$0.06^{+0.03}_{-0.03}$	$6.70^{+0.01}_{-0.01}$	$0.07^{+0.02}_{-0.01}$	$1.76^{+0.02}_{-0.02}$	$5.98^{+0.03}_{-0.03}$	–2.45	3468.24/3256

Column (1): The observation ID; Col. (2): The observation date; Col. (3): The fitting model (A: pha(pow); B: pha*gabs1*gabs2(pow+laor); C: pha*gabs1*gabs2(pexrav+laor)); Col. (4): The column density of neutral hydrogen gas; Cols. (5) and (6): The energy and line width of the absorption line around 7.0 keV; Cols. (7) and (8): The energy and line width of second absorption lines; Col. (9): X-ray photon index (Γ); Col. (10): The central energy of the broad iron emission line; Col. (11): 2–10 keV X-ray scaled Eddington ratio; Col. (12): The reduced χ^2 value.
‡: The BH mass of NGC 1365, $\log(M_{\rm BH}/M_\odot)$, is 6.65, which is adopted from Onori et al. (2017).

The results of joint observations are also presented in Table 1.

3 RESULTS

In the spectral modeling of NGC 1365, we adopted an absorbed power-law component (POW), an iron Kα line and two gaussian absorption iron lines around 6.7 keV and 7.0 keV (GABS). Due to that the BH of NGC 1365 is suggested to be high spin, we adopted the relativistic iron Kα line model (LAOR, Laor 1991), where the inclination angle of 60°, the inner disk radius of $R_{\rm in} = 1.74 R_{\rm g}$ (corresponding to the innermost stable orbit of $a_* = 0.97$) and the emissivity index of $q = 3.0$ were fixed following the joint analysis of XMM-Newton and NuSTAR data (Risaliti et al. 2013). As an example, we present the contour map of $\Gamma - N_{\rm H}$ for an XMM-Newton observation (ID:0692840501) and the joint fitting with the simultaneous observation with NuSTAR (ID:60002046009) in Figure 1, where the fitting results are roughly consistent with each other (i.e., within several percent; see also Table 1). The absorption lines at 6.70 keV and 7.05 keV are evident in seven of the eight observations except for the lowest flux case (ObsID:0151370101), where the average widths are 0.06 ± 0.01 keV and 0.10 ± 0.06 keV respectively based on the gaussian fitting (see Fig. 2). The absorption line at 6.70 keV is evident while the line in 7.0 keV is roughly absent in the observation of 0692840201. It should be noted that two additional weak absorption lines at around 7.80 keV and 8.20 keV are also present in observations of 0205590401 and 0692840301. These two weak lines were not included in our fitting, which are weak and do not affect our modeling results.

In Figure 3, we present the relations of $N_{\rm H} - L_{\rm 2-10keV}/L_{\rm Edd}$ and $\Gamma - L_{\rm 2-10keV}/L_{\rm Edd}$ for the eight observations. It is clear that the column density decreases as the X-ray luminosity increases (left panel) and the X-ray spectral index is positively correlated with the Eddington-scaled X-ray luminosity (right panel). For comparison, we also present the relation of $\Gamma - L_{\rm 2-10keV}/L_{\rm Edd}$ for three other type 1 AGNs with strong variability of X-ray emission from the literatures (NGC 4151 from Zoghbi et al. 2019; NGC 4051 from Lamer et al. 2003; NGC 3516 from de Marco et al. 2009), where the BH masses of $10^{7.6} M_\odot$, $10^{6.3} M_\odot$ and $10^{7.5} M_\odot$ are adopted for NGC 4151, NGC 4051 and NGC 3516, respectively (Grier et al. 2013). The positive X-ray spectral evolution in NGC 1365 is similar to other variable type 1 AGNs even though each of them may follow its own evolutionary track.

The UV luminosities (simultaneous with X-ray data) were also available from the optical monitor (OM) onboard XMM-Newton. We adopted the UVW1 emission at 2675 Å (2410-3565 Å) for six selected observations from Hernández-García et al. (2017), where the UVW1 luminosity and optical-to-X-ray spectral index ($\alpha_{\rm OX}$, calculated from the 2 keV X-ray flux and UVW1 flux) are also listed in Table 2. We present the relations of $L_{\rm UVW1} - L_{\rm 2-10keV}$ and $\alpha_{\rm OX} - L_{\rm UVW1}/L_{\rm Edd}$ in the left

Table 2 The Luminosity of Ultraviolet, X-ray Band and UV/X-ray Spectral Index Data of NGC 1365

ObsID	Date	$\log(L_{2-10})$ ($\rm ergcm^{-2}s^{-1}$)	$\log(L_{UVW1})$ ($\rm ergcm^{-2}s^{-1}$)	$\alpha_{\rm OX}$
(1)	(2)	(3)	(4)	(5)
0205590301	2004-Jan-17	$42.34^{+0.01}_{-0.01}$	$41.69^{+0.01}_{-0.01}$	$0.77^{+0.02}_{-0.02}$
0205590401	2004-Jul-24	$42.02^{+0.01}_{-0.01}$	$42.21^{+0.01}_{-0.01}$	$1.21^{+0.03}_{-0.03}$
0692840201	2012-Jul-25	$42.10^{+0.01}_{-0.01}$	$42.01^{+0.01}_{-0.01}$	$1.12^{+0.02}_{-0.02}$
0692840301	2012-Dec-24	$42.38^{+0.01}_{-0.01}$	$41.94^{+0.01}_{-0.01}$	$0.92^{+0.01}_{-0.01}$
0692840401	2013-Jan-23	$42.33^{+0.01}_{-0.01}$	$41.78^{+0.01}_{-0.01}$	$0.87^{+0.01}_{-0.01}$
0692840501	2013-Feb-12	$42.25^{+0.01}_{-0.01}$	$41.77^{+0.01}_{-0.01}$	$0.92^{+0.01}_{-0.01}$

Column (1): The observation ID; Col. (2): The observing date; Col. (3): The X-ray luminosity in 2–10 keV; Col. (4): The luminosity of UV band at UVW1 band; Col. (5): UV/X-ray spectral index between 2 keV of X-ray band and UVW1 of ultraviolet band.

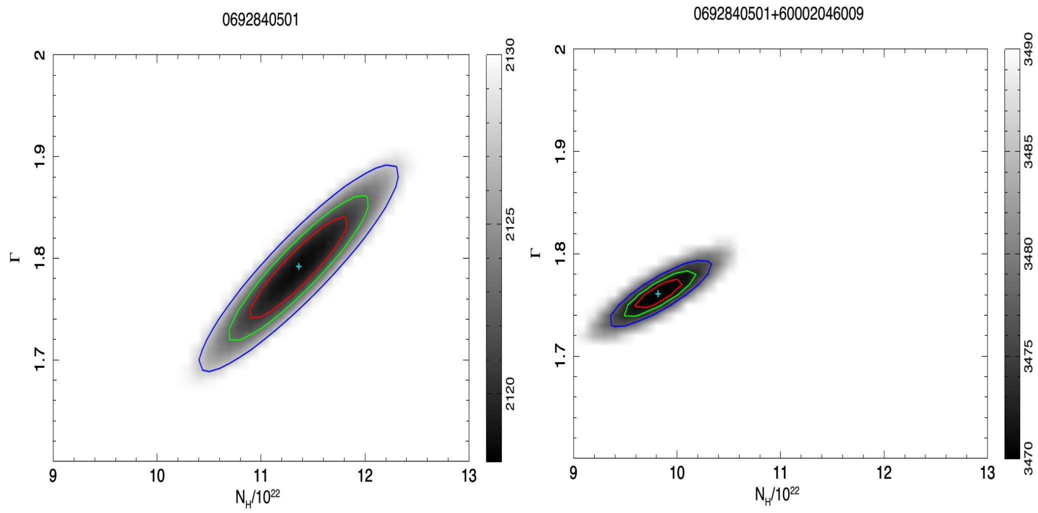

Fig. 1 The contour maps of Γ and $N_{\rm H}$ derived using the XMM-Newton observations (*left*) and the joint simultaneous observations of XMM-Newton and NuSTAR (*right*), where the *blue*, *green* and *red curves* represent the contour levels with 1 σ, 2 σ and 3 σ, respectively. The *color bars* indicate the χ^2 values.

and right panels of Figure 4, where they follow negative and positive correlations, respectively.

4 DISCUSSIONS

NGC 1365 is a Seyfert 1.8 with a highly complex variable absorption and variable X-ray spectrum. The fitting results from the pure XMM-Newton in 3-10 keV band and the joint observations of XMM-Newton/NuSTAR in 3-78 keV bands for four cases as selected suggest that the modeling results should be reasonable even from the pure XMM-Newton observations if $N_{\rm H} < 2 \times 10^{23} \rm cm^{-2}$ (see Fig. 1). The X-ray photon index cannot be well constrained if $N_{\rm H} > 10^{24} \rm cm^{-2}$ based on the pure XMM-Newton observations, where the spectrum should be reflection-dominated. In this work, we mainly focus on the evolution of X-ray spectral index, and, therefore, adopt a simple model in fitting the data within 3-10 keV band. It should be noted that the multiple absorption components may exist in NGC 1365, which mainly contribute at low energy band (e.g., 0.5-2 keV). Our fitting result is roughly consistent with that fitting with multi-layer variable absorber model (e.g., the differences for photon index are less than 10%, Rivers et al. 2015). The different fitting models will not affect the evolutionary trends.

4.1 Evolution of Γ and $\alpha_{\rm OX}$: Evidence for Disk Evolution

It was found that the X-ray photon index, Γ, is strongly correlated with the Eddington ratio, $L_{\rm bol}/L_{\rm Edd}$, in both X-ray binaries and AGNs, where the X-ray photon index is negatively and positively correlated with the Eddington ratio when $L_{\rm bol}/L_{\rm Edd}$ is lower and higher than a critical value of $\sim 10^{-2}$, respectively (e.g., Wang et al. 2004; Yuan et al. 2007; Wu & Gu 2008; Trichas et al. 2013; Yang et al. 2015, and references therein). The optically-selected

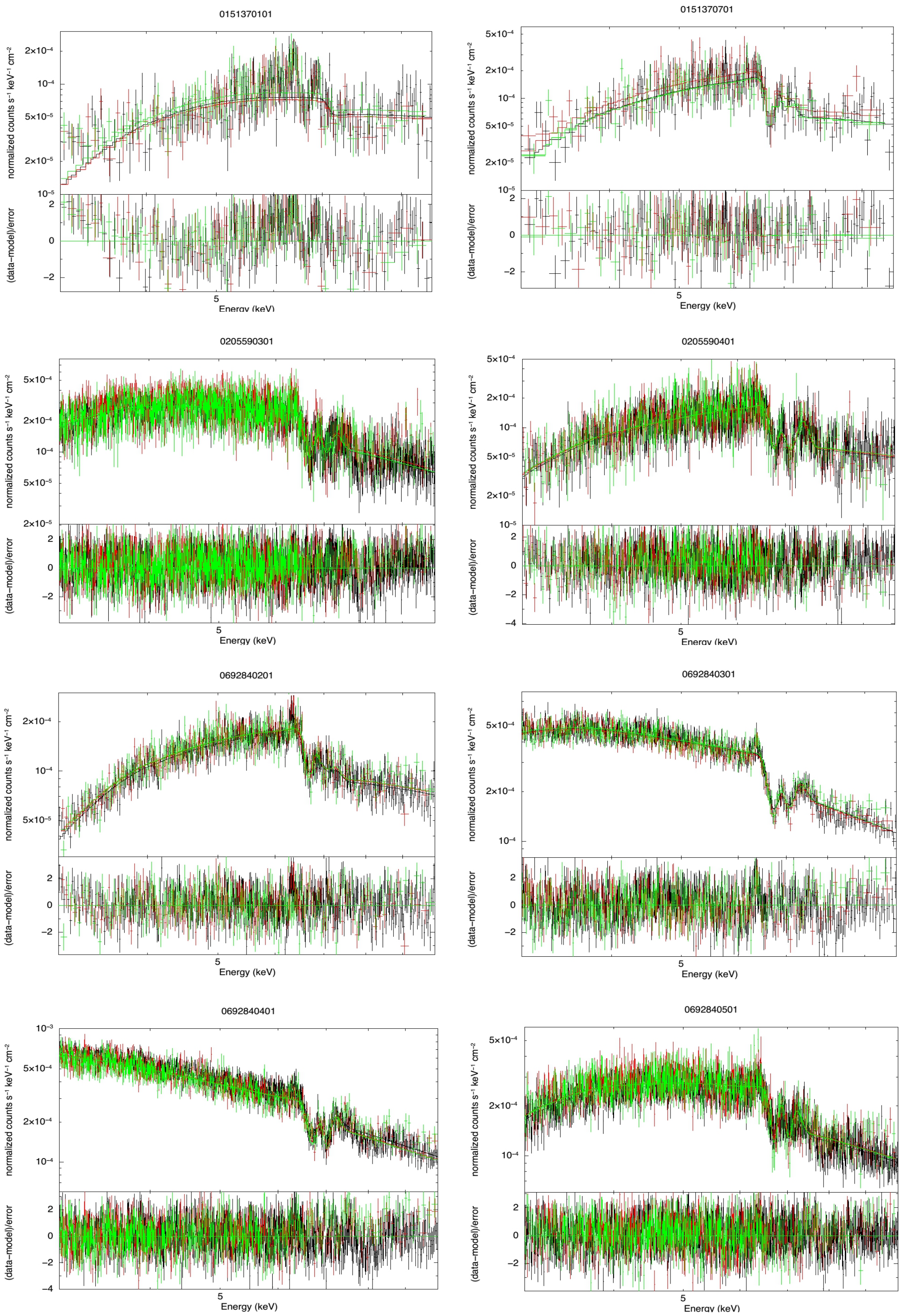

Fig. 2 The spectral fitting results for the eight XMM-Newton observations. The *black*, *red* and *green points* represent the data of PN instrument, MOS1 and MOS2 instruments, respectively.

CL AGNs with reappearance and disappearance of broad lines displayed a remarkable similarity as that found in both X-ray binaries and AGNs (e.g., Noda & Done 2018; Ruan et al. 2019; Ai et al. 2020). The positive correlations

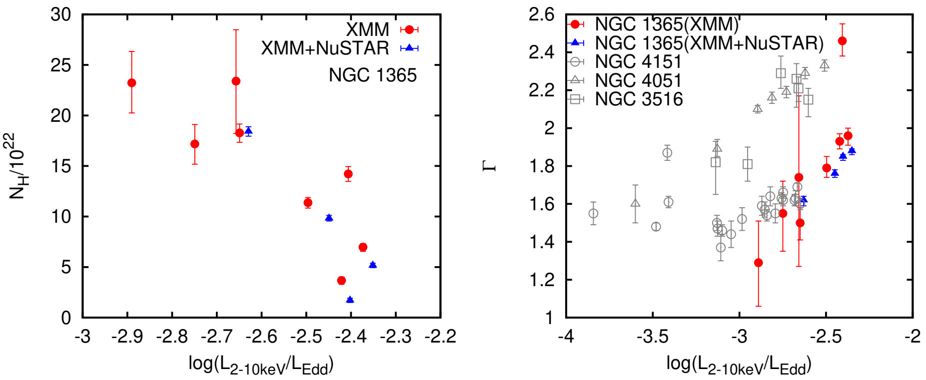

Fig. 3 Left panel: The correlation between $N_{\rm H}$ and $\log(L_{2-10\rm keV}/L_{\rm Edd})$ for NGC 1365. For comparison, we present the fitting results for XMM-Newton (*red circles*) and the joint analysis of XMM-Newton/NuSTAR (*blue triangles*). Right panel: The correlation of $\Gamma - \log(L_{2-10\rm keV}/L_{\rm Edd})$, and we also present the correlation for other three variable AGNs.

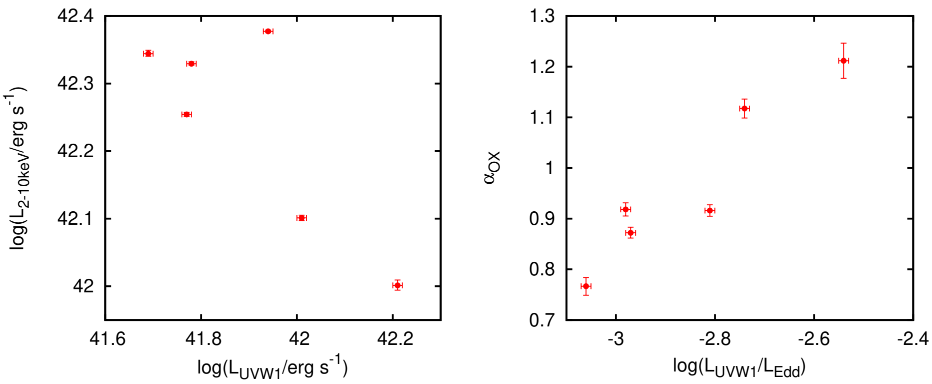

Fig. 4 The left panel and right panel represent the relations of $L_{2-10\ \rm keV} - L_{\rm UVW1}$ and $\alpha_{\rm OX} - \log(L_{\rm UVW1}/L_{\rm Edd})$, respectively.

of $\Gamma - L_{2-10\rm keV}/L_{\rm Edd}$ as found in NGC 1365 are quite consistent with other optically-selected CL AGNs in bright states and/or bright AGNs (Lusso et al. 2010; Weng et al. 2020; Zhu et al. 2020). In NGC 1365, the column density is anti-correlated with the X-ray luminosity (see also Connolly et al. 2014; Rivers et al. 2015), indicating less absorption at higher X-ray luminosities. The correlation between $\alpha_{\rm OX}$ and $L_{\rm UVW1}/L_{\rm Edd}$ also follows a positive correlation, which is also consistent with that found in other bright AGN samples (e.g., Xu 2011; Ruan et al. 2019, and references therein). However, it should be noted that the UV emission may be underestimated due to the putative torus and/or the optically thick winds. The positive correlation of $\alpha_{\rm OX} - L_{\rm UVW1}/L_{\rm Edd}$ will not change even considering the possible absorption. The physical reason is that the higher optical/UV emission corresponds to the lower X-ray emission (see the left panel of Fig. 4) and higher absorption column density (see the left panel of Fig. 3), which means that the intrinsic optical emission should be stronger compared with the observed optical flux. Therefore, the data points will move up and right direction in the right panel of Figure 4. The possible absorption correction for the optical emission can further test this relation, which is beyond the scope of this work. Both the X-ray and optical emission is varied only 2–3 times, and the strong evolution of X-ray spectrum suggests the strong mass exchange between the cold disk and the hot corona, which often happens at $L_{\rm bol}/L_{\rm Edd} \sim 1\%$. This phenomenon is also found in a changing-look LINER (low-ionization nuclear emission-line region galaxy, ZTF18aajupnt, Frederick et al. 2019).

The negative and positive correlations of spectral evolution for both pure X-ray and the UV to X-ray spectral indexes may correspond to different accretion modes, respectively. For the case of $L_{\rm bol}/L_{\rm Edd} > 1\%$, the cold disk can extend to the innermost stable orbit (Fig. 3). More plasma will be cooled down into the thin disk as increasing of accretion rate, then the coronal optical depth will decrease and lead to a softer X-ray spectrum (i.e., the positive correlation, Cao 2009; You et al. 2012; Qiao & Liu 2013; Yang et al. 2015). In the low-accretion-rate scenario (e.g., $L_{\rm bol}/L_{\rm Edd} < 1\%$), the inner cold disk may evaporate into the hot accretion flow (e.g., advection dominated accretion flow, ADAF), and the optical depth of the hot plasma will increase as increasing of accretion rate, which will lead to a harder X-ray spectrum (i.e., the negative correlation). The UV/X-ray spectral index $\alpha_{\rm OX}$ also follows negative and positive correlations when the Eddington ratio is below and above a critical rate (e.g., Xu 2011; Ruan et al. 2019). The positive correlations of $\Gamma - L_{\rm 2-10keV}/L_{\rm Edd}$ and $\alpha_{\rm OX} - L_{\rm UVW1}/L_{\rm Edd}$ in NGC 1365 are consistent with the spectral behavior of AGNs and X-ray binaries at the high-accretion rate stage, where the cold disk should exist (e.g., Figs. 3 and 4, Ruan et al. 2019). The bolometric Eddington ratio of NGC 1365 is around several percent if assuming that the typical bolometric correction factor is $\sim$ 10 in 2-10 keV band or $\sim$ 5 in optical-UV band (e.g., Duras et al. 2020), which is slightly larger than the critical Eddington ratio of $\sim 1\%$ for the possible disk transition. In this stage, the cold disk and corona strongly evolve through evaporation and condensation (e.g., Liu et al. 2015).These results suggest that the accretion process in NGC 1365 should be similar to other optically-selected CL AGNs and its accretion disk may change dramatically, where the bolometric Eddington ratio is around 1% and the accretion disk normally experiences strong evolution.

4.2 Evolution of $N_{\rm H} - L_{\rm 2-10keV}/L_{\rm Edd}$: Variable Column Density Triggered by the Evolved Accretion Disk?

The column density varies within several months or even several hours in NGC 1365, which suggests that the absorbing material should be clumpy and at a much smaller distance than the conventional obscuring torus. The disk winds can be served as the mechanism for the variable column density and absorprtion lines (Proga & Kallman 2004; Sim et al. 2010; Tombesi et al. 2012; Gofford et al. 2015; Miller et al. 2016; Braito et al. 2021), which can be driven by radiation pressure etc. (e.g., King & Pounds 2015; You et al. 2016; Li & Cao 2019). The anti-correlation of $N_{\rm H} - L_{\rm 2-10keV}/L_{\rm Edd}$ or $N_{\rm H} - \Gamma$ suggest that the absorption material most possibly correlated with the accretion process (see left and right panels in Fig. 3). As the accretion rate decreases, the radiation pressure will decrease and part of winds cannot escape (e.g., failed winds), which will lead to more dense clouds near the black hole or higher column densities. The other possibility for the anti-correlation of column density and luminosity is that the expanding or shrinking of corona in the polar axis. Couto et al. (2016) proposed that the average column density will decrease as the expanding of the corona and increasing of luminosity, which is also applicable to X-ray binaries (Kara et al. 2019; You et al. 2021, for MAXI J1820+070). The black hole X-ray binary GRS 1915+105 went into a dim state after 26 years in outburst, where the source shows evidence of persistently increasing internal obscuration and a reduced mass accretion rate (see fig. 3 and fig. 6 in Neilsen et al. 2020; Balakrishnan et al. 2020), which is similar to the CL AGN of NGC 1365. The failed winds maybe the physical reason for the variation of absorption material in different-scale of BH systems.

Even though we find the evidence for the possible state transition in an X-ray selected CL AGN NGC 1365 based on the X-ray spectral evolution, it is still unclear whether other X-ray selected CL AGNs share the similar physical mechanism or not. The disk winds may be a mechanism for producing the clouds that move in and out of our line of sight. More analyses with multi-waveband observations for the CL AGNs with variable column density are needed to further test this scenario, which will be presented in a future work.

5 CONCLUSIONS

Over last several years, increasing evidence has shown that the reappearance and disappearance of broad emission lines in CL AGNs may be triggered by the change of the accretion process. It is still unclear what physical mechanism is at work for the AGNs with extreme variable column density, even though they were originally defined as CL AGNs. Based on the spectral analyses of the CL AGN NGC 1365 with strong variations of column density, we find that:

(1) The X-ray spectrum and optical-to-X-ray spectral index show strong evolution as increasing of X-ray luminosity, where both $\Gamma - L_{\rm 2-10keV}/L_{\rm Edd}$ and $\alpha_{\rm OX} - L_{\rm UVW1}/L_{\rm Edd}$ follow positive correlations. These results suggest that the disk and corona should strongly evolve in NGC 1365, which follow a similar state transition as found in X-ray binaries and other optically-selected CL AGNs.

(2) The variable $N_{\rm H}$ and the anti-correlation of $N_{\rm H} - L_{\rm 2-10keV}/L_{\rm Edd}$ as observed in NGC 1365 suggest that the absorption should be closely correlated with the accretion process, which may be regulated by the disk wind.

Acknowledgements We appreciate the useful discussions with Wu Xuebing, Yu Wenfei, Cao Xinwu, You Bei. Q. Wu and H. Liu acknowledge support from the National Natural Science Foundation of China (NSFC, Grant No. U1931203). Y.Q. Xue acknowledges support from NSFC (Grant Nos. 12025303, 11890693 and 11421303), the CAS Frontier Science Key Research Program (QYZDJ-SSW-SLH006), and the K.C. Wong Education Foundation. Z.-C. He is supported by NSFC (Grant No. 11903031) and USTC Research Funds of the Double First-Class Initiative YD 3440002001. H. Guo is supported by NSF grant AST1907290.

References

Ai, Y., Dou, L., Yang, C., et al. 2020, ApJ, 890, L29
Antonucci, R. 1993, ARA&A, 31, 473

Balakrishnan, M., Miller, J. M., Trueba, N., et al. 2020, ApJ, 893, 155
Braito, V., Reeves, J. N., Severgnini, P., et al. 2021, MNRAS, 500, 291
Cao, X. 2009, MNRAS, 394, 207
Connolly, S. D., McHardy, I. M., & Dwelly, T. 2014, MNRAS, 440, 3503
Couto, J. D., Kraemer, S. B., Turner, T. J., & Crenshaw, D. M. 2016, ApJ, 833, 191
de Marco, B., Iwasawa, K., Cappi, M., et al. 2009, A&A, 507, 159
Denney, K. D., De Rosa, G., Croxall, K., et al. 2014, ApJ, 796, 134
Duras, F., Bongiorno, A., Ricci, F., et al. 2020, A&A, 636, A73
Edmunds, M. G., & Pagel, B. E. J. 1982, MNRAS, 198, 1089
Fausnaugh, M. M., Starkey, D. A., Horne, K., et al. 2018, ApJ, 854, 107
Frederick, S., Gezari, S., Graham, M. J., et al. 2019, ApJ, 883, 31
Gofford, J., Reeves, J. N., McLaughlin, D. E., et al. 2015, MNRAS, 451, 4169
Goodrich, R. W. 1989, ApJ, 340, 190
Grier, C. J., Martini, P., Watson, L. C., et al. 2013, ApJ, 773, 90
Guo, H., Sun, M., Liu, X., et al. 2019, ApJ, 883, L44
Guo, H., Peng, J., Zhang, K., et al. 2020, ApJ, 905, 52
Hernández-García, L., Masegosa, J., González-Martín, O., et al. 2017, A&A, 602, A65
Hutsemékers, D., Agís González, B., Marin, F., et al. 2019, A&A, 625, A54
Kara, E., Steiner, J. F., Fabian, A. C., et al. 2019, Natur, 565, 198
Kim, D.-C., Yoon, I., & Evans, A. S. 2018, ApJ, 861, 51
King, A., & Pounds, K. 2015, ARA&A, 53, 115
Lamer, G., McHardy, I. M., Uttley, P., & Jahoda, K. 2003, MNRAS, 338, 323
Laor, A. 1991, ApJ, 376, 90
Li, J., & Cao, X. 2019, ApJ, 886, 92
Liu, B. F., Taam, R. E., Qiao, E., & Yuan, W. 2015, ApJ, 806, 223
Lusso, E., Comastri, A., Vignali, C., et al. 2010, A&A, 512, A34
MacLeod, C. L., Ross, N. P., Lawrence, A., et al. 2016, MNRAS, 457, 389
MacLeod, C. L., Green, P. J., Anderson, S. F., et al. 2019, ApJ, 874, 8
Mathur, S., Denney, K. D., Gupta, A., et al. 2018, ApJ, 866, 123
McElroy, R. E., Husemann, B., Croom, S. M., et al. 2016, A&A, 593, L8
Miller, J. M., Raymond, J., Fabian, A. C., et al. 2016, ApJ, 821, L9
Neilsen, J., Homan, J., Steiner, J. F., et al. 2020, ApJ, 902, 152
Noda, H., & Done, C. 2018, MNRAS, 480, 3898
Onori, F., Ricci, F., La Franca, F., et al. 2017, MNRAS, 468, L97
Planck Collaboration, Ade, P. A. R., Aghanim, N., et al. 2014, A&A, 571, A16
Proga, D., & Kallman, T. R., 2004, ApJ, 616, 688
Qiao, E., & Liu, B. F. 2013, ApJ, 764, 2
Ramos, A., C., Levenson, N. A., Rodríguez Espinosa, J. M., et al. 2009, ApJ, 702, 1127
Ricci, C., Bauer, F. E., Arevalo, P., et al. 2016, ApJ, 820, 5
Risaliti, G., Miniutti, G., Elvis, M., et al. 2009, ApJ, 696, 160
Risaliti, G., Harrison, F. A., Madsen, K. K., et al. 2013, Nature, 494, 449
Rivers, E., Markowitz, A., Duro, R., & Rothschild, R. 2012, ApJ, 759, 63
Rivers, E., Risaliti, G., Walton, D. J., et al. 2015, ApJ, 804, 107
Ruan, J. J., Anderson, S. F., Cales, S. L., et al. 2016, ApJ, 826, 188
Ruan, J. J., Anderson, S. F., Eracleous, M., et al. 2019, ApJ, 883, 76
Schulz, H., Komossa, S., Schmitz, C., & Mucke, A. 1999, A&A, 346, 764
Schnorr-Müller, A., Davies, R. I., Korista, K. T., et al. 2016, MNRAS, 462, 3570
Sheng, Z., Wang, T., Jiang, N., et al. 2017, ApJ, 846, L7
Sim, S. A., Proga, D., Miller, L., Long, K. S., & Turner, T. J. 2010, MNRAS, 408, 1396
Śniegowska, M., & Czerny, B. 2019, arXiv, arXiv:1904.06767
Tombesi, F., Cappi, M., Sambruna, R. M., et al. 2012, ASPC, 460, 8
Trakhtenbrot, B., Arcavi, I., MacLeod, C. L., et al. 2019, ApJ, 883, 94
Tran, H. D., Osterbrock, D. E., & Martel, A. 1992, AJ, 104, 2072
Trichas, M., Green, P. J., Constantin, A., et al. 2013, ApJ, 778, 188
Trippe, M. L., Crenshaw, D. M., Deo, R., & Dietrich, M. 2008, AJ, 135, 2048
Trippe, M. L., Crenshaw, D. M., Deo, R. P., et al. 2010, ApJ, 725, 1749
Urry, C. M., & Padovani, P. 1995, PASP, 107, 803
Walton, D. J., Risaliti, G., Harrison, F. A., et al. 2014, ApJ, 788, 76
Wang, J.-M., Watarai, K.-Y., & Mineshige, S. 2004, ApJ, 607, L107
Wang, J., Fabbiano, G., Elvis, M., et al. 2009, ApJ, 694, 718
Wang, J.-M., & Bon, E. 2020, A&A, 643, L9
Weng, S.-S., Chen, Y., Wang, T.-T., et al. 2020, MNRAS, 491, 2576
Wu, Q., & Gu, M. 2008, ApJ, 682, 212
Xu, Y.-D. 2011, ApJ, 739, 64
Yang, Q.-X., Xie, F.-G., Yuan, F., et al. 2015, MNRAS, 447, 1692
Yang, Q., Wu, X.-B., Fan, X., et al. 2018, ApJ, 862, 109
You, B., Cao, X., & Yuan, Y.-F. 2012, ApJ, 761, 109
You, B., Straub, O., Czerny, B., et al. 2016, ApJ, 821, 104
You, B., Tuo, Y., Li, C., et al. 2021, NatCo, 12, 1025
Yuan, F., Taam, R. E., Misra, R., et al. 2007, ApJ, 658, 282
Zhu, S. F., Brandt, W. N., Luo, B., et al. 2020, MNRAS, 496, 245
Zoghbi, A., Miller, J. M., & Cackett, E. 2019, ApJ, 884, 26